A Comparison Study of Multidirectional Waves Generated in Laboratory Basins

M.D. MILES[1], M. BENOIT[2], P. FRIGAARD[3],
P.J. HAWKES[4], H.A. SCHÄFFER[5] and C.T. STANSBERG[6]

[1] Canadian Hydraulics Centre, Ottawa, Canada
[2] Laboratoire National d'Hydraulique, Chatou, France
[3] Aalborg University, Aalborg, Denmark
[4] HR Wallingford, Oxfordshire, UK
[5] Danish Hydraulic Institute, Hørsholm, Denmark
[6] Marintek, Trondheim, Norway

Abstract

This paper describes the results of a comparison study that was carried out by the IAHR working group on multidirectional waves. Multidirectional waves were generated in six different laboratory basins according to specified target directional wave spectra for both broad and narrow spreading functions. The measured waves were then analysed by a common MEM (maximum entropy) method to investigate the variability due to different wave synthesis and generation methods. Numerical simulations were also performed to evaluate the effects of wave diffraction and reflection.

1 Introduction

Due to increasing interest in the use of multidirectional waves for physical model tests in hydraulics laboratories, the Maritime Hydraulics Section of the IAHR formed a working group on multidirectional waves in 1994 (Briggs, 1997). Two of the tasks carried out by this working group were comparison studies of the generation and analysis methods that are typically used for the reproduction and measurement of multidirectional wave fields in laboratory basins using segmented wave machines. The first study (Hawkes et al., 1997) compared the results of different wave analysis methods on common sets of synthesized and measured directional wave data. This paper presents the results of the second study which used a common analysis method to compare multidirectional waves that were generated and measured in several different laboratory basins.

The desired multidirectional wave conditions for a model test are usually specified by a directional wave spectrum $S(f, \theta) = S_\eta(f) \cdot D(f, \theta)$ where $S_\eta(f)$ is the frequency spectrum of the wave elevation $\eta(t)$ and $D(f, \theta)$ is a directional spreading function, which may vary with frequency. Starting from this specification, the following steps are typically carried out to produce the required waves in a model basin:

1. If necessary, the target frequency spectrum and spreading function are first adjusted to comply with the essential constraints of the wave generator and the basin (maximum wave frequency, minimum and maximum wave angles, etc.).

2. A particular pseudo-random wave field of specified duration is synthesized according to the modified target frequency spectrum and spreading function.

3. The wave generator paddle motions required to generate the pseudo-random wave field are computed (usually by linear wave theory) in accordance with the side boundary conditions of the basin. These paddle motions may also include compensation for other effects, such as, wave machine servo dynamics, spectral matching based on previous measurements, etc.

4. The wave field is generated in the basin and measured by an array of sensors.

5. Directional wave analysis is performed to estimate the frequency spectrum and spreading function of the measured waves.

6. The measured wave spectrum and spreading function are compared to the desired targets and steps 3 to 6 are repeated until a satisfactory match is obtained.

The actual multidirectional waves obtained will vary from one basin to another due to differences in the procedures listed above and differences in basin configurations and equipment. The primary objective of this study was to investigate variability in the reproduction of typical directional wave spectra in laboratory basins due to differences in wave synthesis, generation and measurement methods. Each participating laboratory synthesized and generated three test cases according to their standard operational methods and measured the resulting waves at a specified location with a specified array of wave sensors. The measured time series wave data from the various basins were then analysed by a common procedure to eliminate variations caused by different directional wave analysis methods. The resulting directional spectra were then compared to investigate the variability due to differences in wave basin equipment and generation methods. Thus, this study was designed to complement the first study (Hawkes et al., 1997) which investigated the variability due to different directional wave analysis methods.

The total variability depends on numerous factors associated with the different wave generation methods. Due to the expense of conducting tests in multidirectional wave basins and the limited number of participating laboratories, the physical wave tests could provide useful information on the overall variability but could not be used to assess the relative influence of individual factors. Consequently, it was decided to also carry out some numerical modelling of a typical wave basin equipped with a segmented wave generator. Since certain individual factors could be easily controlled in the numerical model, it was used to assess the relative influence of factors such as wave diffraction and reflection in the basin. The numerical model results would also be useful for interpreting the results from the physical wave generation tests.

2 Wave Synthesis and Generation Methods

Sand and Mynett (1987) contains a very good overview of the synthesis and generation methods that are typically used to produce multidirectional waves in laboratory basins. Wave synthesis generally consists of defining a pseudo-random wave field of specified duration that represents a particular realization of a natural sea state defined by a given directional spectrum, $S(f, \theta)$. The resulting wave field usually consists of the superposition of several hundred or several thousand sinusoidal wave components with individual amplitudes, phases and directions of propagation set according to a particular wave synthesis model.

The two most commonly used synthesis models are the double summation model and the single summation model. The double summation model contains wave components with many different directions at each frequency whereas the single summation model has only one wave direction at each frequency. The main advantage of the single summation model is that the resulting wave field is spatially homogeneous for the durations that are typically used for model tests. In contrast, the double summation model only becomes spatially homogeneous for very long record durations. The relative merits of the single and double summation models are discussed in Jefferys (1987) and Miles and Funke (1989). These two basic synthesis models can also be implemented in several different ways. For example, the discrete frequencies can either be uniformly spaced for FFT operations or non-harmonic frequencies can be used. One example of the non-harmonic approach is the equal energy method in which the spectrum is divided into bands of equal energy and each band is represented by sinusoidal components of equal amplitude with random phase angles. In the harmonic approach, the amplitudes and phases of the sinusoidal components can either be set by the random phase method or by the random Fourier coefficient method. Similarly, the discrete wave angles can either be uniformly spaced or selected at random according to the cumulative distribution of the target spreading function. Thus, when comparing multidirectional waves generated in different laboratory basins, a certain degree of variability can

be expected due to the many different factors involved in synthesizing a wave field for a given directional wave spectrum.

Once the wave field has been synthesized, there are several different wave generation methods that can be used to calculate the wave machine paddle motions required to generate it in a particular basin. These are usually based on linear wave theory and the most commonly used technique is the Snake Principle method, as described in Sand and Mynett (1987). This method is straightforward to implement and is well proven. Its main disadvantage is that the useful working area in the basin is quite limited by diffraction unless segmented wave machines are installed on more than one side of the basin. Other directional wave generation methods include the diffraction method (Naesser, 1979), the directional filter method (Bryden and Greated, 1984) and a second order method (Suh and Dalrymple, 1987) but these have not been commonly used.

HR Wallingford have developed a unique short-crested wave generation technique called the method of mode spectra (Gilbert and Huntington, 1991). This method uses full-length reflecting side walls and the total directional spectrum is produced by superimposing about 50 mode spectra with discrete wave numbers k_y corresponding to the natural cross modes of the basin. This technique provides a much larger homogeneous working area (about 50% of the basin width) than the Snake Principle method but it is restricted to symmetric spreading functions with the mean wave direction normal to the segmented wave generator.

Another effective technique for increasing the useful working area in a basin has been developed by Dalrymple (1989). This method can produce an oblique regular wave component across the full width of the basin at a specified distance from the wave generator by using intentional reflection from full-length or partial length side walls. This method can be easily extended by superposition to produce random short-crested seas with a much larger useful working area than the standard Snake Principle method.

The essential physical constraints of each particular basin and wave generator must also be considered when generating a multidirectional wave field. For example, the minimum and maximum wave angles that can be generated at the test site are usually limited by diffraction effects and basin geometry. It may be necessary to truncate and re-normalize the target spreading function to stay within these limits. At higher frequencies, the maximum wave angle that can be generated depends on the segment width of the wave machine according to the Biesel limit (Biesel, 1954). This limit must be enforced to prevent spurious wave generation in the basin. This can be done either by truncating the frequency spectrum or by limiting the spreading width at higher frequencies. At DHI, such spurious waves are prevented by not generating a component unless $a_1/a_0 < \epsilon$ where a_1 is the maximum spurious wave amplitude and a_0 is the primary wave amplitude. Some other practical techniques for dealing with physical constraints are described in Cornett et al. (1993).

Differences in these various wave generation methods and procedures for dealing with constraints will also contribute to the variability when a given directional spectrum is generated in different laboratory basins.

3 Test Cases

Six test cases were selected based on the primary tests cases A1 and B1 that were used for the companion comparison study of directional wave analysis methods (Hawkes et al., 1997). The various parameters for these test cases are listed in Table 1 where s and θ_0 are the parameters of the following target directional spreading function:

$$D(\theta) = \frac{\Gamma(s+1)}{2\sqrt{\pi}\,\Gamma(s+0.5)} \cos^{2s}\left((\theta - \theta_0)/2\right) \tag{1}$$

In Table 1, d is the water depth and x_c is the distance from the centre wave probe to the wave generator. The target spectrum for all cases is a JONSWAP with $\gamma = 3.3$.

Test	T_p	H_{m0}	θ_0	s	d	x_c	Comments
P1	1.8 s	12 cm	0°	6	3.0 m	8.0 m	Standard test, deep water
P2	1.8 s	6 cm	0°	6	0.5 m	3.0 m	Standard test, shallow water
Q1	1.8 s	12 cm	0°	40	3.0 m	8.0 m	Narrow spread, deep water
Q2	1.8 s	6 cm	0°	40	0.5 m	3.0 m	Narrow spread, shallow water
R1	1.8 s	24 cm	0°	6	3.0 m	8.0 m	Larger amplitude, deep water
R2	1.8 s	12 cm	0°	6	0.5 m	3.0 m	Larger amplitude, shallow water

Table 1: Test cases for multidirectional waves to be generated in laboratory basins

Two versions of each of the three primary P, Q and R cases were defined for depths of 0.5 m and 3.0 m because most of the available basins were restricted to either deep or shallow water. The wave amplitudes for cases P and Q were chosen to be within the linear range. Case R is case P with the wave height doubled to investigate the effects of increased wave steepness.

A standard sensor configuration was specified for measuring the waves generated in each basin. This consisted of a symmetric array of 6 wave elevation probes with an optional 2-axis current meter, as shown in Figure 1. The current meter measured the horizontal velocity components u and v at the same (x, y) position as wave probe 6. This sensor configuration is the same as that used in the companion study on wave analysis methods and allows the directional spectra to be estimated either

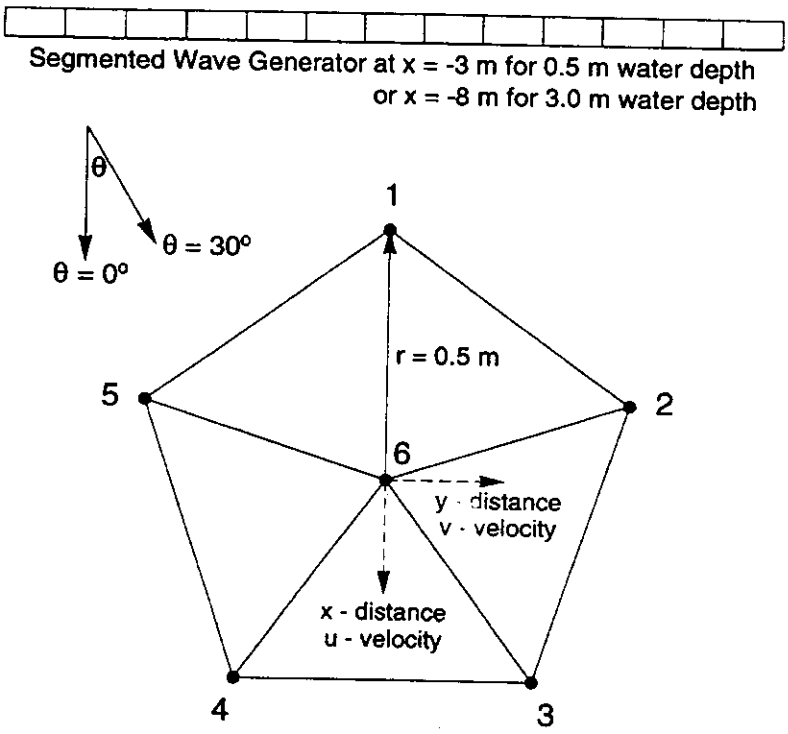

Figure 1: Standard wave probe array configuration

by the (η, u, v) method or by the wave probe array method. Each participating laboratory was requested to generate as many of these test cases as it could with the time series data measured for a duration 1500 seconds.

4 Wave Analysis Methods

The measured time series data from each laboratory were sent to the Canadian Hydraulics Centre (CHC) for directional wave analysis by a common method. The directional spectra were then estimated by using programs MEMVL and MEMWP which are the standard programs used at CHC for routine analysis of multidirectional wave data. These programs are both based on the Maximum Entropy (MEM) Method. Program MEMVL computes the directional wave spectrum from time series of $\eta(t)$, $u(t)$ and $v(t)$ measured at the same (x, y) position. It is based on the method described in Nwogu et al. (1987). Program MEMWP computes the directional spectrum from time series of $\eta(t)$ measured at 4 to 8 different (x, y) positions and is based on the method described in Nwogu (1989).

Programs MEMVL and MEMWP both employ a standard FFT technique that uses the full record length to compute the various cross spectra required and then use the MLM method to compute the initial estimate for the iterative MEM procedure. Both programs are based on the assumption of a spatially homogeneous wave field and do not include any special provisions to handle phase locking effects due to local reflecting boundaries.

In addition to the spreading function $D(f, \theta)$, MEMVL and MEMWP also compute the mean wave direction $\theta_m(f)$ and the spreading width $\sigma_\theta(f)$ for the main incident wave field by integrating over an angular range from $\theta_p - \pi/2$ to $\theta_p + \pi/2$ where $\theta_p(f)$ is the wave angle corresponding to the main peak of $D(f, \theta)$. This procedure is used to minimize the effects of any reflected waves in the basin on the estimates of $\theta_m(f)$ and $\sigma_\theta(f)$ for the main incident wave system.

5 Numerical Simulations

Some numerical simulations were first carried out using the CHC WAGEN5 numerical model. WAGEN5 is an extended version of the WAGEN linear boundary element diffraction model described in Isaacson and Mathai (1993). It can be used to predict the wave fields produced by one or more segmented wave generators in a basin of constant depth. The basin may also contain any combination of fully reflecting walls or partially reflecting passive wave absorbers. The wave generators can also be modelled either with or without active wave absorption capability. The WAGEN numerical model, upon which WAGEN5 is based, has been previously verified by wave basin experiments (Hiraishi et al., 1992).

WAGEN5 was used to simulate the waves produced in a typical 20 m by 30 m wave basin with a 60-segment wave generator installed along one 30 m side and passive absorbers installed on the other three sides. The target wave field was first synthesized by the single summation method with random wave angles and the corresponding wave machine paddle motions were calculated by the standard Snake Principle method. The WAGEN5 numerical model was then used with linear superposition to compute the irregular multidirectional wave field that would be produced in the basin by these paddle motions. The effects of wave diffraction and reflection could be studied independently by specifying different reflection coefficients for the passive absorbers in the simulations.

Numerical simulations were run for test cases P1 and Q1 with a water depth of 3.0 m. Since WAGEN5 is a linear model, it was not necessary to run a separate simulation for test case R1 because the results would be the same as case P1. In each case, the synthesized waves had 2048 Fourier components with random phases and directions to obtain a non-repetitive duration of 1500 seconds at a frequency resolution of 0.0006667 Hz.

The maximum wave angle that can be generated by a segmented machine installed on one side of a basin is limited by geometrical constraints. The theoretical spreading functions were truncated at ± 70 deg. and re-normalized to comply with this constraint. In test case P1, this truncation resulted in a target spreading width of $\sigma_\theta = 29.5$ deg. which is slightly less than the theoretical value of $\sigma_\theta = 31.7$ deg. for the original spreading function. Due to the narrower spreading, this truncation had no significant effect on test case Q1.

Four contour plots of the normalized significant wave height from the numerical simulations of Test Cases P1 and Q1 are shown in Figure 2. These plots show the significant wave height produced at each position in the basin divided by the significant wave height of the desired target wave spectrum. The segmented wave generator is located along the Y axis as indicated by the row of black and white squares in these plots. Passive absorbers with reflection coefficient C_R were installed on the other three sides of the basin. Each case was first run with $C_R = 0.0$ to determine the effects of wave diffraction alone in a basin with perfect absorbers. Each case was then run a second time with $C_R = 0.2$ to study the influence of reflected waves. A standard segmented wave machine without active wave absorption was used in all cases so the wave generator acted as a fully reflecting wall for any waves reflected back from the other three sides of the basin.

The contour plots in Figure 2 provide a good indication of the useful working area in the basin where the multidirectional wave field is reasonably homogeneous. The white circle marked point A on these plots shows the specified location of the wave probe array to be used for these test cases. Plots 2a and 2c show the effects of diffraction and plots 2b and 2d show the combined effects of diffraction and reflection. The diffraction effects are greater for case P1 due to its wider spreading. The main wave reflection effects occur at x values greater than 10 m and are more severe for case Q1 since it has narrower spreading than case P1.

One advantage of the WAGEN5 numerical model is that the wave field is completely defined at all points in the basin by potential functions $\Phi_j(x, y, z)$ for the various incident and reflected wave components. Consequently, the directional properties can be computed directly from these potentials without having to resort to any particular analysis method (such as MLM, MEM, Bayesian, etc.) to estimate them. The mean wave angle θ_m and the spreading width σ_θ were both computed directly from the potential functions and the results are shown in the contour plots in Figures 3 and 4. The $\theta_m(x, y)$ and $\sigma_\theta(x, y)$ data shown in these plots are average values for the incident wave field obtained by integrating over a range of wave angles from $-\pi/2$ to $+\pi/2$ and over the frequency range from 0.4 to 1.0 Hz with weighting function $S_\eta(f)$.

Figure 3 shows the relative influence of wave diffraction and reflection on θ_m at different locations in the basin. Wave diffraction generally causes much larger variations in θ_m than wave reflection. The main effects occur near the two sides of the basin at y = 0 and y = 30 m and are larger for case P1 than case Q1. In the centre region of the basin in the vicinity of point A, neither diffraction nor reflection has a significant effect on θ_m when it is calculated over the angular range from $-\pi/2$ to $+\pi/2$ corresponding to the incident wave field.

The effects of diffraction and reflection on the spreading width σ_θ are shown in Figure 4. It can be seen that diffraction has a much greater influence than wave reflections in both test cases. As one would expect, the diffraction effects are greater for case P1 and the reflection effects are larger for case Q1. In all four

cases shown in Figure 4, the σ_θ values in the vicinity of point A are quite close to the target values of 29.5 and 12.7 degrees for test cases P1 and Q1, respectively.

Time series data were also generated from the numerical simulations for the wave sensor configuration shown in Figure 1 with the centre wave probe (no. 6) and the (u, v) current meter located at point A in the basin. These time series data were then processed by the same MEMVL and MEMWP programs that were used to analyze the measured data from the laboratory basin tests, as described in Section 6. The time series records were 1500 seconds long and the MEM analysis was performed at a frequency resolution of 0.04 Hz. The following three sets of time series data were analyzed for each of the P1 and Q1 test cases:

SYN	The wave field synthesized by the single summation method with random wave angles for the target directional spectrum. This synthesized wave field is homogeneous over the entire (x, y) plane and is not related to any particular basin.
GEN1	The generated wave field at point A in the 20 by 30 m basin as computed by the numerical model for the case of a 60-segment wave generator on one side and perfect wave absorbers ($C_R = 0.0$) on the other 3 sides.
GEN2	The generated wave field at point A in the 20 by 30 m basin as computed by the numerical model for the case of a 60-segment wave generator on one side and partially reflecting wave absorbers ($C_R = 0.2$) on the other 3 sides.

The resulting $D(\theta)$ spreading functions from the MEM analysis of these data sets for test cases P1 and Q1 are shown in Figures 5 and 6. These plots show the spreading function $D(f, \theta)$ at $f = f_p$ and the average spreading function computed as follows:

$$\text{Average } D(\theta) = \frac{\int_{f_1}^{f_2} S_\eta(f) \cdot D(f, \theta)\, df}{\int_{f_1}^{f_2} S_\eta(f)\, df} \tag{2}$$

where $f_1 = 0.4$ Hz and $f_2 = 1.0$ Hz.

It can be seen in Figure 5 that the SYN and GEN1 spreading functions are almost identical in all cases so wave diffraction has very little effect at point A. The GEN2 spreading functions have a slightly narrower main peak and broad secondary peak at 180 deg. due to the reflected waves. The average SYN $D(\theta)$ matches the target spreading function very closely for the (η, u, v) data but is slightly narrower than the target for 6 probe array data.

The average SYN and GEN1 $D(\theta)$ results for case Q1 also match the target spreading function very closely, as shown in Figure 6. As expected, the GEN2

spreading functions for this case have a narrow secondary peak at 180 deg. due to wave reflection.

The mean wave direction $\theta_m(f)$ and the spreading width $\sigma_\theta(f)$ computed by the MEM analysis programs are plotted as functions of frequency for test case P1 in Figure 7. The target wave spectrum $S_\eta(f)$ is also included in the background of these plots to indicate the relative wave energy available at each frequency for estimating $\theta_m(f)$ and $\sigma_\theta(f)$. The SYN, GEN1 and GEN2 results all show very similar variability with frequency and match the target values quite well on average. These results clearly show that most of the variability with frequency is caused by the wave synthesis method itself and not by diffraction and reflection in the basin. Even with the relatively long duration of 1500 seconds (model scale), the single summation method only has about 70 random wave angles in each 0.04 Hz frequency band which accounts for most of the variability shown in Figure 7. This variability in $\theta_m(f)$ and $\sigma_\theta(f)$ can be reduced by using equally spaced angles instead of random angles in the single summation method, but only at the expense of increased variability in the frequency spectrum (Miles, 1989).

It should also be noted that although diffraction and reflection have little effect at point A, this is not true at other positions in the basin. Results were also computed for case GEN3 which is the same as GEN2 except that the wave data were computed at point B instead of point A where point B is located at $(x, y) = (16, 23)$ m in the basin. As can be seen from the GEN3 results in Figure 7, diffraction and reflection can have a large influence on $\theta_m(f)$ and $\sigma_\theta(f)$, depending on the location in the basin.

The corresponding $\theta_m(f)$ and $\sigma_\theta(f)$ results for test case Q1 are shown in Figure 8. The variability with frequency is only about half as large as case P1 due to the narrower spreading function. As in case P1, the SYN and GEN1 results have very similar variability but the GEN2 σ_θ results for the 6 probe array data show increased variability due to wave reflection. Since wave reflection increases spatial inhomogeneity, it has a greater influence on the spatially-separated 6 probe array results than on the spatially-coincident η, u, v results.

6 Wave Basin Tests

The physical wave generation tests for this study were performed at the following six laboratories:

Aalborg University, Aalborg, Denmark
Canadian Hydraulics Centre, Ottawa, Canada
Danish Hydraulic Institute, Hørsholm, Denmark
HR Wallingford, Oxfordshire, UK
Laboratoire National d'Hydraulique, Chatou, France
Marintek, Trondheim, Norway

Laboratory	Water Depth	Cases Performed	η, u, v data	6-probe array
Lab 1	0.5 m	P2, Q2, R2	yes	yes
Lab 2	3.0 m	P1, Q1, R1	yes	yes
Lab 3	0.5 m	P2, Q2, R2	no	yes
Lab 4	0.5 m	P2, Q2, R2	yes	yes
Lab 5	3.0 m	P1, Q1, R1	no	yes
Lab 6	0.5 m	P2, Q2, R2	no	yes

Table 2: Test cases performed at each laboratory

Since the objective was to investigate overall variability without regard to individual basins, the various sets of wave data have been given designations of Lab 1 to Lab 6 with the numbers 1 to 6 assigned in no particular order. The lab numbers used in this paper also have no particular correspondence to those in Hawkes et al. (1997).

The test cases performed at each laboratory are listed in Table 2. The waves were synthesized and generated by the standard operational methods normally used in each laboratory. The waves were then measured using the standard instrumentation in each laboratory with the various wave sensors configured as shown in Figure 1. Data were collected from each sensor at a 20 Hz sampling rate for a duration of 1500 seconds. The resulting time series data were then sent to the Canadian Hydraulics Centre for analysis by the MEMVL and MEMWP programs described in Section 4. The directional wave analysis was carried out at a frequency resolution of 0.04 Hz.

Since only six sets of data were available, it was not possible to evaluate the effects of different water depths. Consequently, the data from the six test cases P1, P2, Q1, Q2, R1 and R2 have been merged into three test cases designated P, Q and R for the purpose of comparing results from the various laboratory basins.

After performing the directional analysis, it was also discovered that the Lab 3 waves had not been generated for the correct target spreading functions. A target spreading function of the form $\cos^n(\theta)$ had been used with n values of 6 and 40 instead of the specified $\cos^{2s}(\theta/2)$ spreading function with s values of 6 and 40. Consequently, the target σ_θ values for the Lab 3 waves were actually 21.6 deg. for test cases P and R and 9.0 deg. for test case Q instead of the specified values of 31.7 deg. for cases P and R and 12.7 deg. for case Q. The target θ_m values for the Lab 3 data were correct. Unfortunately, it was not possible to schedule the Lab 3 basin to repeat the tests with the correct target spreading functions. Since only six sets of data were available for this comparison study, it was decided to retain the Lab 3 results as much as possible while noting the different target spreading widths that had been used to generate these particular waves.

The average $D(\theta)$ spreading functions computed by Equation 2 from the MEM analysis results for each set of laboratory data are plotted in Figures 9, 10 and 11 for test cases P, Q and R, respectively. These spreading functions have been averaged over the main frequency range from $f_1 = 0.4$ Hz to $f_2 = 1.0$ Hz. The $D(f, \theta)$ spreading functions at the spectral peak frequency $f = f_p$ are also shown in these figures.

The average $D(\theta)$ results for test case P (broad spreading) in Figure 9 show very good agreement with the target spreading function for all of the (η, u, v) data sets. There is slightly greater variability between the laboratory data sets for the 6-probe array data but the overall agreement is still very good. The Lab 1 results also have a broad secondary peak at 180 deg. for the (η, u, v) case but not for the 6-probe array case. As one would expect, the $D(f, \theta)$ results at frequency $f = f_p$ have greater variability than the average $D(\theta)$ spreading functions but the overall agreement with target spreading function is still reasonably good for both the (η, u, v) results and the 6-probe array results. The Lab 3 results have not been included in Figures 9 and 11 because their target spreading width was significantly narrower than the specified target for test cases P and R.

The average $D(\theta)$ results for test case Q (narrow spreading) in Figure 10 also show very good agreement with the target spreading function for all of the (η, u, v) data sets. The average $D(\theta)$ results for the 6-probe array data have greater variability for test case Q than for test case P. The overall agreement is still quite good although the average $D(\theta)$ for Lab 6 is noticeably broader than the other results. The Lab 1 results have a small secondary peak at $\theta = 180$ deg. in all four plots in Figure 10 which was probably caused by wave reflection from the opposite side of the basin. Some of the results from the other laboratories also have broader secondary peaks near 180 deg. which may indicate some reflected wave activity in the basins. The Lab 3 results have been included in Figure 10 since the target spreading width was only 3.7 degrees narrower than the specified target for this case. The Lab 3 results have the narrowest average $D(\theta)$ which is probably due to the slightly narrower target spreading that was used to generate these waves.

The wave amplitudes specified for test cases R1 and R2 were chosen to produce waves on the verge of breaking. When these cases were run, some of the laboratories did not observe any breaking waves while others reported only a few breaking waves at various positions in the basin. As shown in Figure 11, the overall agreement of the average $D(\theta)$ results with the target spreading function is very good for all of the test case R results. In general, the spreading function results for test case R are very similar to those for test case P. Thus, the increased wave steepness did not seem to have a significant effect on the directional wave characteristics. The 6-probe array results for $D(f, \theta)$ at $f = f_p$ actually have somewhat smaller variability for test case R than for test case P. This may be due to smaller relative measurement errors in the wave probe data when the wave amplitude is increased.

The mean wave direction $\theta_m(f)$ and the spreading width $\sigma_\theta(f)$ are plotted as functions of frequency for Test Case P in Figure 12. The target frequency spectrum $S_\eta(f)$ has also been included in the background of these plots for reference. The target values for θ_m and σ_θ are also shown by dashed lines on these plots. Although the theoretical spreading width is 31.7 deg. for test case P, the target σ_θ value has been set to 29.5 deg. which corresponds to truncating the theoretical spreading function at ± 70 degrees to comply with the minimum and maximum wave angles that can typically be generated at the test site in the various participating wave basins.

The various laboratory data sets generally show similar levels of variability with frequency. The accuracy of the (η, u, v) results tends to decrease somewhat with increasing frequency which may be due to increased noise in the current meter measurements at higher frequencies. Most of the results agree quite well with the target values on average. As noted previously, the Lab 3 waves were generated for a different target spreading of $\sigma_\theta = 21.6$ deg. as shown by the short dashed line in Figure 12d. The σ_θ results for Lab 3 are about 5 degrees less than their target value on average but otherwise have similar variability with frequency as the other results.

The corresponding $\theta_m(f)$ and $\sigma_\theta(f)$ results for test case Q are shown in Figure 13. In general, the variability with frequency is smaller than test case P over the main frequency range from 0.4 to 1.0 Hz. The variability of σ_θ for the 6-probe array data is somewhat larger, however. As before, the accuracy of the (η, u, v) results tends to decrease with increasing frequency. The 6-probe array σ_θ results for test case Q are about 3 degrees larger than the target value on average but all of the other test case Q results agree very well with the target values on average. The Lab 3 σ_θ results are about 4 deg. smaller than the other results on average which is consistent with the narrower target spreading that was used to generate these waves.

The $\theta_m(f)$ and $\sigma_\theta(f)$ results for test case R are shown in Figure 14. In general, these results are very similar to those for test case P, as shown in Figure 12. Thus, the increased wave steepness does not have a significant effect on these directional wave parameters.

7 Concluding Remarks

The following general observations can be made by comparing the numerical simulation results in Figures 7 and 8 with the corresponding results from the wave basin tests in Figures 12 and 13:

- The variability of $\theta_m(f)$ and $\sigma_\theta(f)$ is generally smaller for test case Q than for test case P for both the numerical simulations and the laboratory basin

waves. The 6-probe array σ_θ results for the laboratory basin waves are an exception, however, having slightly greater variability for case Q than for case P.

- The accuracy of the (η, u, v) results decreases with increasing frequency for the laboratory basin waves but not the numerical simulations. Since a similar effect does not occur for the 6-probe array data, this is probably associated with high frequency noise in the (u, v) measurements.

- Roughly half of the variability in the laboratory basin results can probably be attributed to wave synthesis effects (including statistical variability). The remaining part is due to other factors, such as, differences in generation methods, wave sensor characteristics, wave generator accuracy, etc.

- The numerical simulation results for test case Q1 indicate that wave reflection effects on σ_θ are greater for the 6-probe array case than the (η, u, v) case. This may account for some of the greater variability in the σ_θ results for the 6-probe array compared to the (η, u, v) data in the test case Q results in Figure 13.

- The numerical simulation results indicate that wave diffraction and reflection effects have relatively minor influence at the specified test location.

In general, the results of this comparison study are rather encouraging and indicate that these types of multidirectional wave fields can be reproduced in laboratory basins with reasonable accuracy and consistency. Most of the laboratory basin results matched the target parameters quite well and the degree of variability obtained does not appear to be excessive in view of the many factors involved in the various wave synthesis and generation methods that were used. It should be noted that the waves were measured near the optimum locations in the basins, however, and that much larger deviations would probably have been obtained at other positions. The results also show that numerical models are an effective tool for determining the useful working area available in a basin when a particular type of multidirectional wave field is being generated.

8 References

Biesel, F., (1954): *Wave Machines*, Proc. of First Conf. on Ships and Waves (Council on Wave Research & SNAME), Hoboken, 1954, pp. 288–304.

Briggs, M., (1997): *IAHR Working Group on Multidirectional Waves: An historical overview*, IAHR Seminar on Multidirectional Waves and their Interaction with Structures, XXVII IAHR Congress, San Francisco.

Bryden, I.G. and Greated, C.A., (1984): *Generation of three-dimensional random waves*, J. Phys. D: Appl. Phys., **17**, pp. 2351–2366.

Cornett, A.M. et al. (1993): *Physical Modelling of Multidirectional Waves*, 2nd Int. Symposium on Ocean Wave Measurement and Analysis, New Orleans.

Dalrymple, R.A., (1989): *Directional Wavemaker Theory with Sidewall Reflection*, Journal of Hydraulic Research, Vol. 27, No. 1, pp. 23–34.

Gilbert, G. and Huntington, S.W., (1991): *A Technique for the Generation of Short Crested Waves in Wave Basins*, Journal of Hydraulic Research, Vol. 29, No. 6, pp. 789–799.

Hawkes, P.J. et al., (1997): *Comparative Analyses of Multidirectional Wave Basin Data*, IAHR Seminar on Multidirectional Waves and their Interaction with Structures, XXVII IAHR Congress, San Francisco.

Hiraishi, T. et al., (1992): *Validation of a Numerical Diffraction Model for Multidirectional Wave Generation*, Proc. 2nd Int. Offshore and Polar Eng. Conf., San Francisco, pp. 154–169.

Isaacson, M. and Mathai, T., (1993): *Wave Field in a Laboratory Wave Basin with Partially Reflecting Boundaries*, Proc. 3rd Int. Offshore and Polar Eng. Conf., Singapore, pp. 669–676.

Jefferys, E.R., (1987): *Directional Seas should be Ergodic*, Applied Ocean Research, **9**, (4), pp. 186–191.

Miles, M.D., (1989): *A Note on Directional Random Wave Synthesis by the Single Summation Method*, Proc. XXIII IAHR Congress, Ottawa, pp. 243–250.

Miles, M.D. and Funke, E.R., (1989): *A Comparison of Methods for Synthesis of Directional Seas*, ASME OMAE Journal, **111**, (1), pp. 43–48.

Naeser, H., (1979): *Generation of Uniform Directional Spectra in a Wave Basin using the Natural Diffraction of Waves*, Proc. POAC, Norway, pp. 621–632.

Nwogu, O.G., (1989): *Maximum Entropy Estimation of Directional Wave Spectra from an Array of Wave Probes*, Applied Ocean Research, **11**, 4, pp. 176–182.

Nwogu, O.G., et al., (1987): *Estimation of Directional Wave Spectra by the Maximum Entropy Method*, IAHR Seminar on Wave Analysis and Generation in Laboratory Basins, XXII IAHR Congress, Lausanne, pp. 363–376.

Sand, S.E., and Mynett, A.E., (1987): *Directional Wave Generation and Analysis*, IAHR Seminar on Wave Analysis and Generation in Laboratory Basins, XXII IAHR Congress, Lausanne, pp. 209–235.

Suh, K. and Dalrymple, R.A., (1987): *Directional Wavemaker Theory: A Spectral Approach*, IAHR Seminar on Wave Analysis and Generation in Laboratory Basins, XXII IAHR Congress, Lausanne, pp. 389–395.

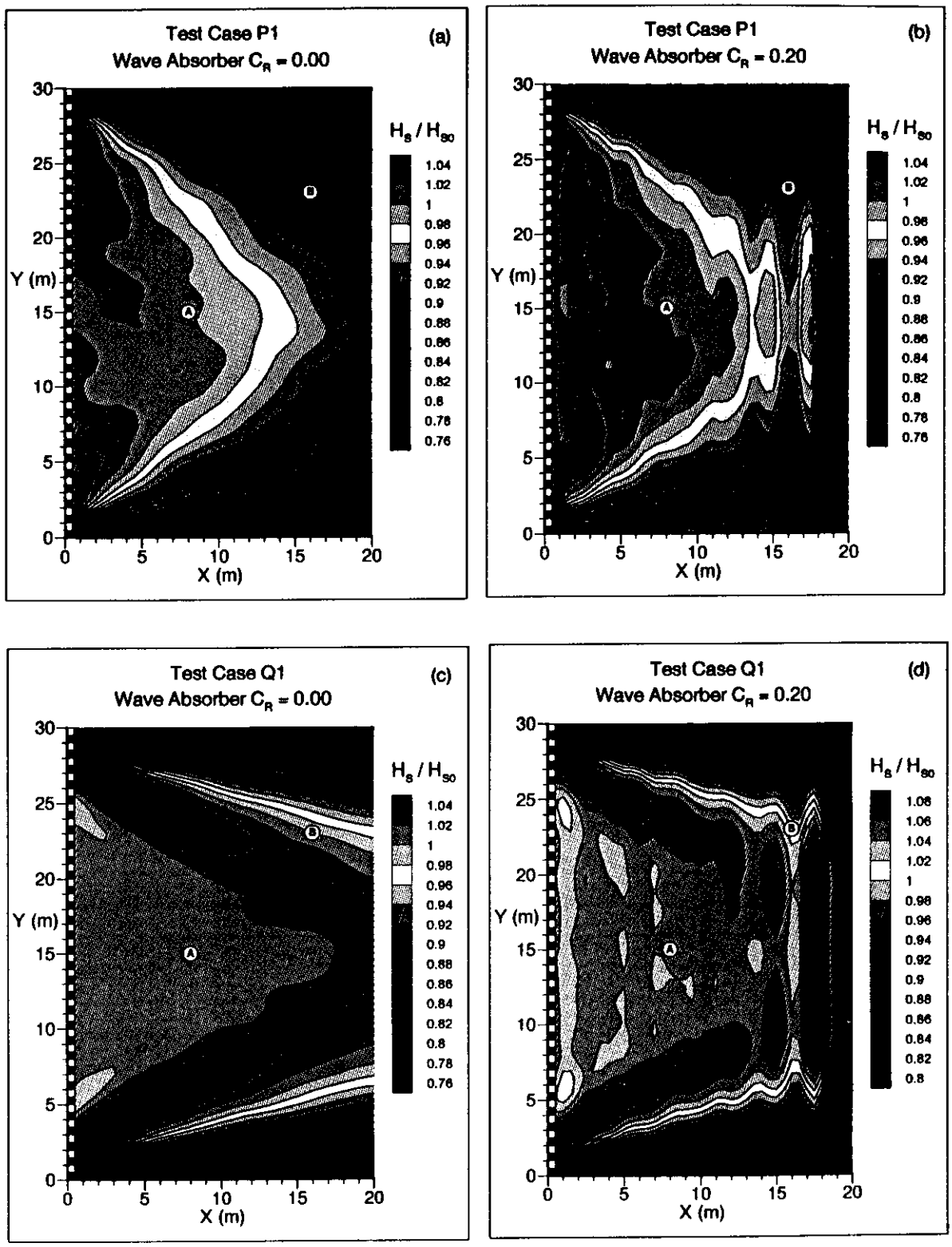

Figure 2: Normalized significant wave height from numerical simulations of Test Cases P1 and Q1

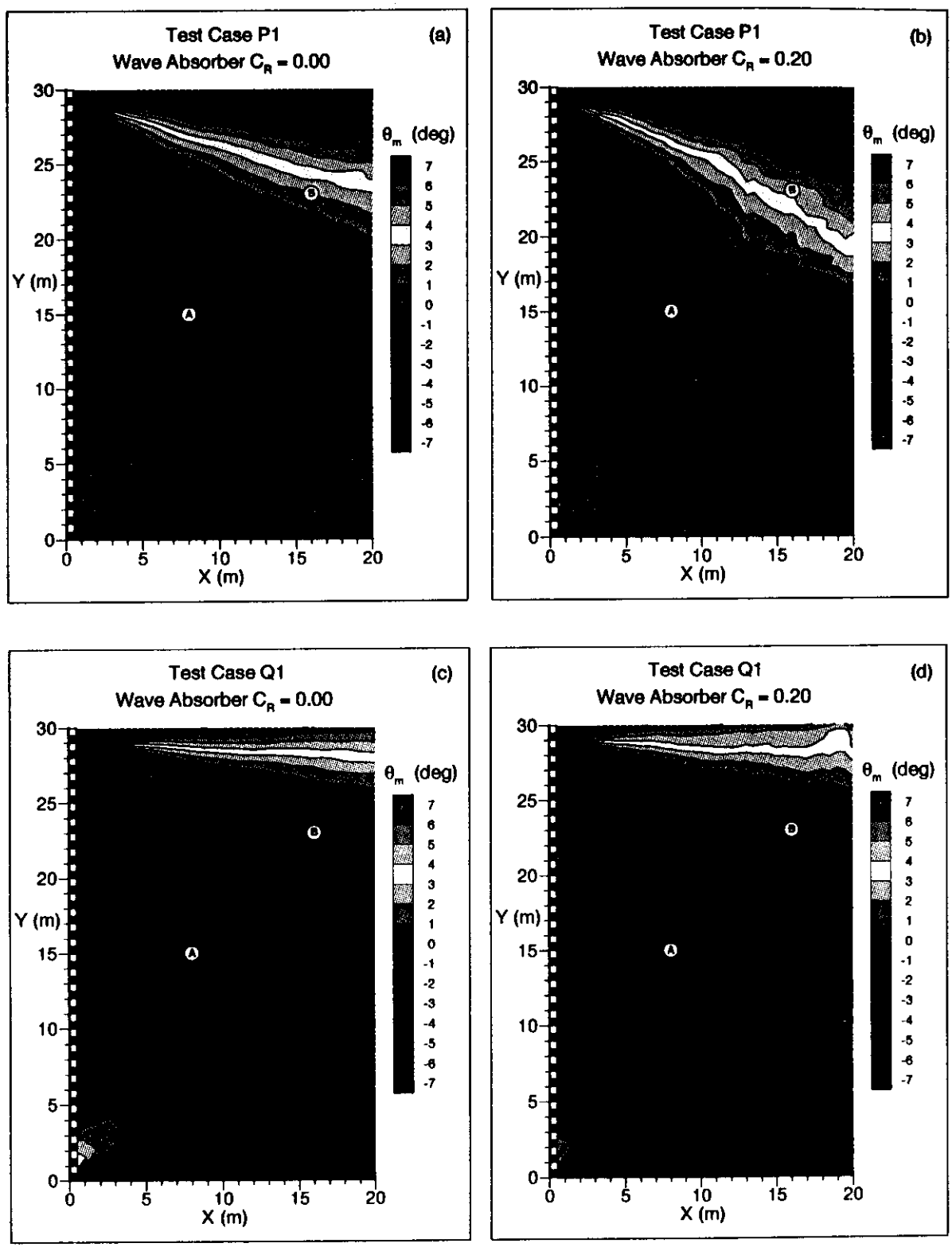

Figure 3: Mean wave direction θ_m for incident wave field from numerical simulations of Test Cases P1 and Q1

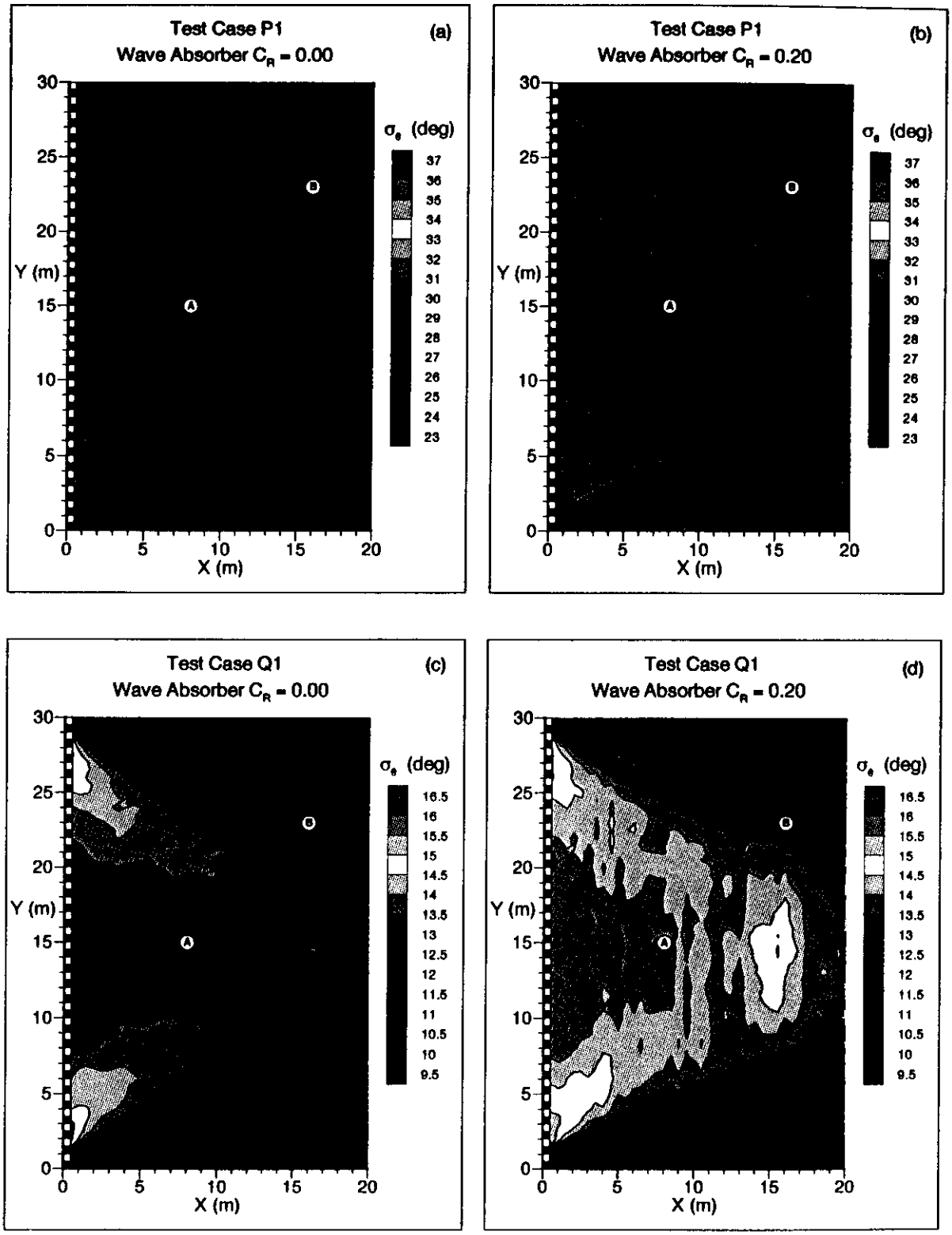

Figure 4: Spreading width σ_θ for incident wave field from numerical simulations of Test Cases P1 and Q1

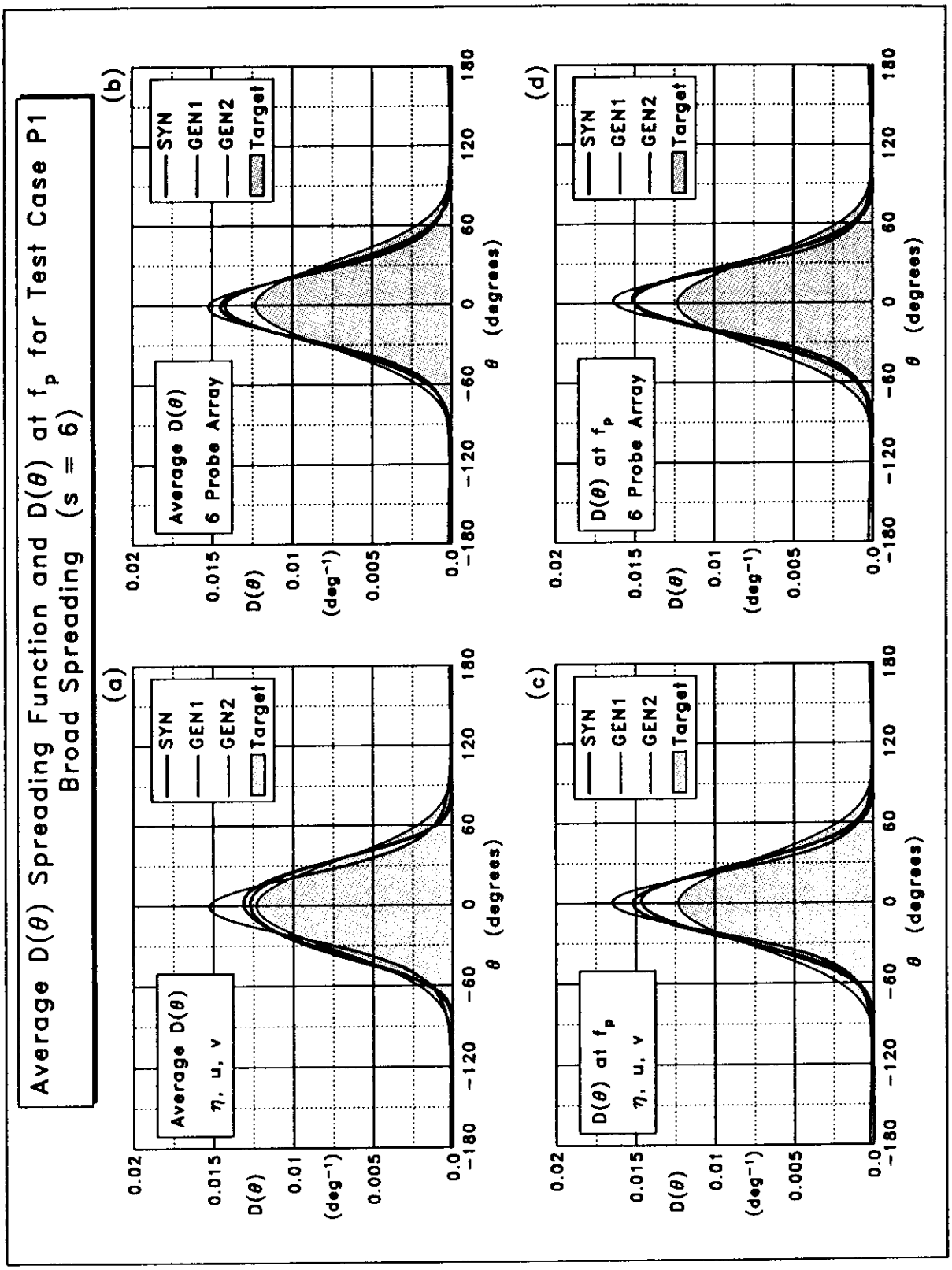

Figure 5: $D(\theta)$ spreading functions computed by programs MEMVL and MEMWP using time series data from numerical simulations of Test Case P1

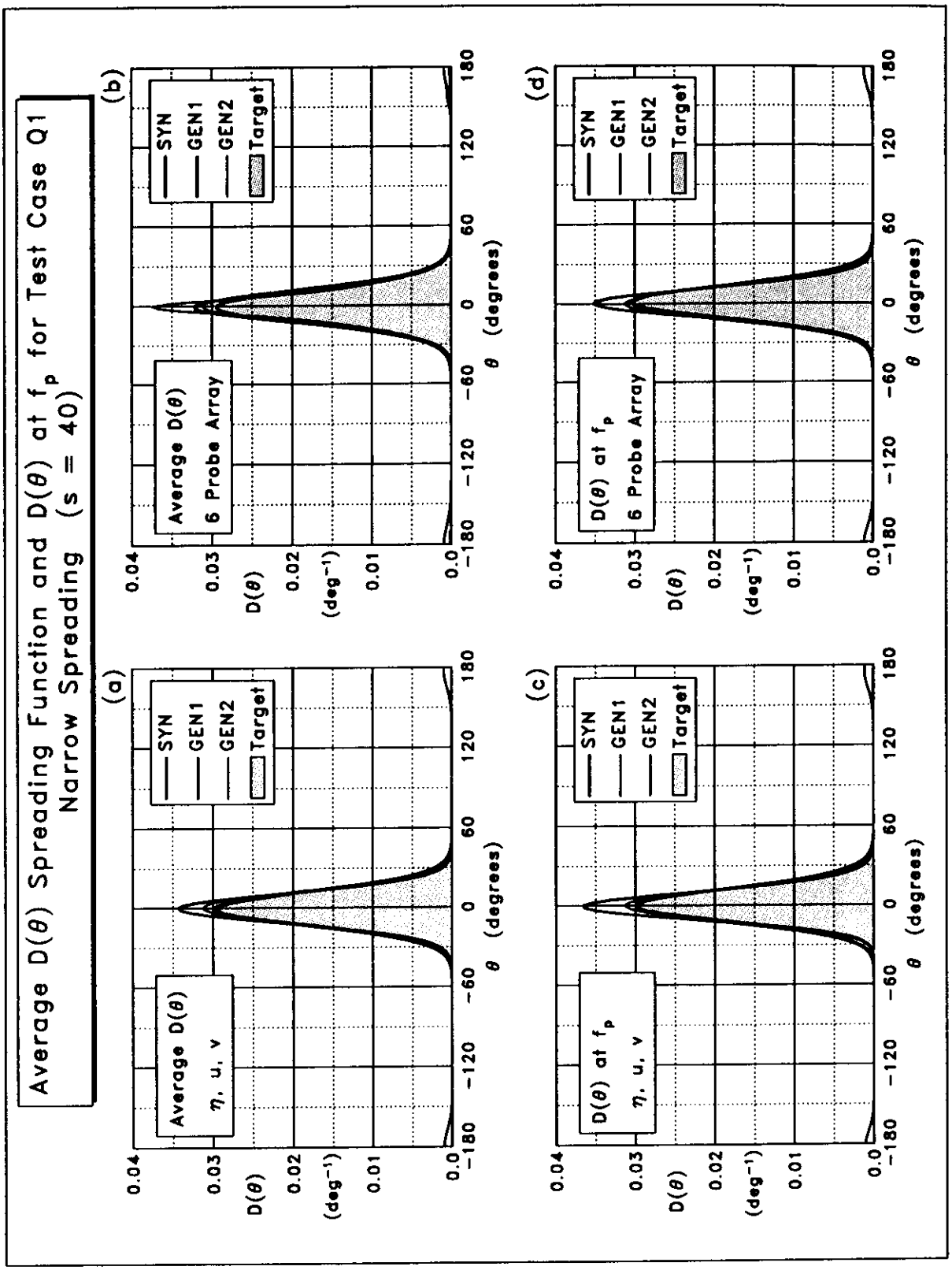

Figure 6: $D(\theta)$ spreading functions computed by programs MEMVL and MEMWP using time series data from numerical simulations of Test Case Q1

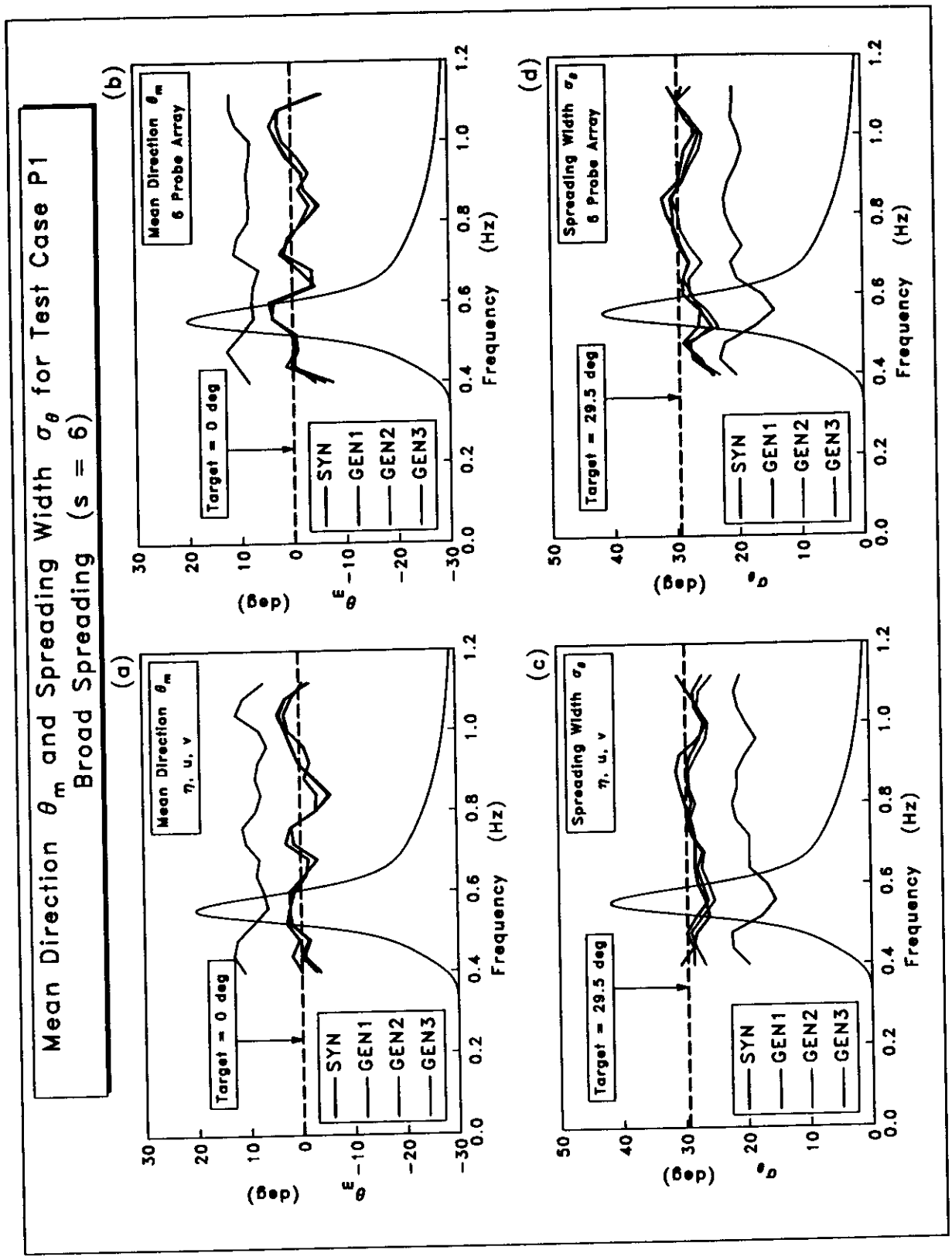

Figure 7: Mean wave direction $\theta_m(f)$ and spreading width $\sigma_\theta(f)$ computed by programs MEMVL and MEMWP using time series data from numerical simulations of Test Case P1

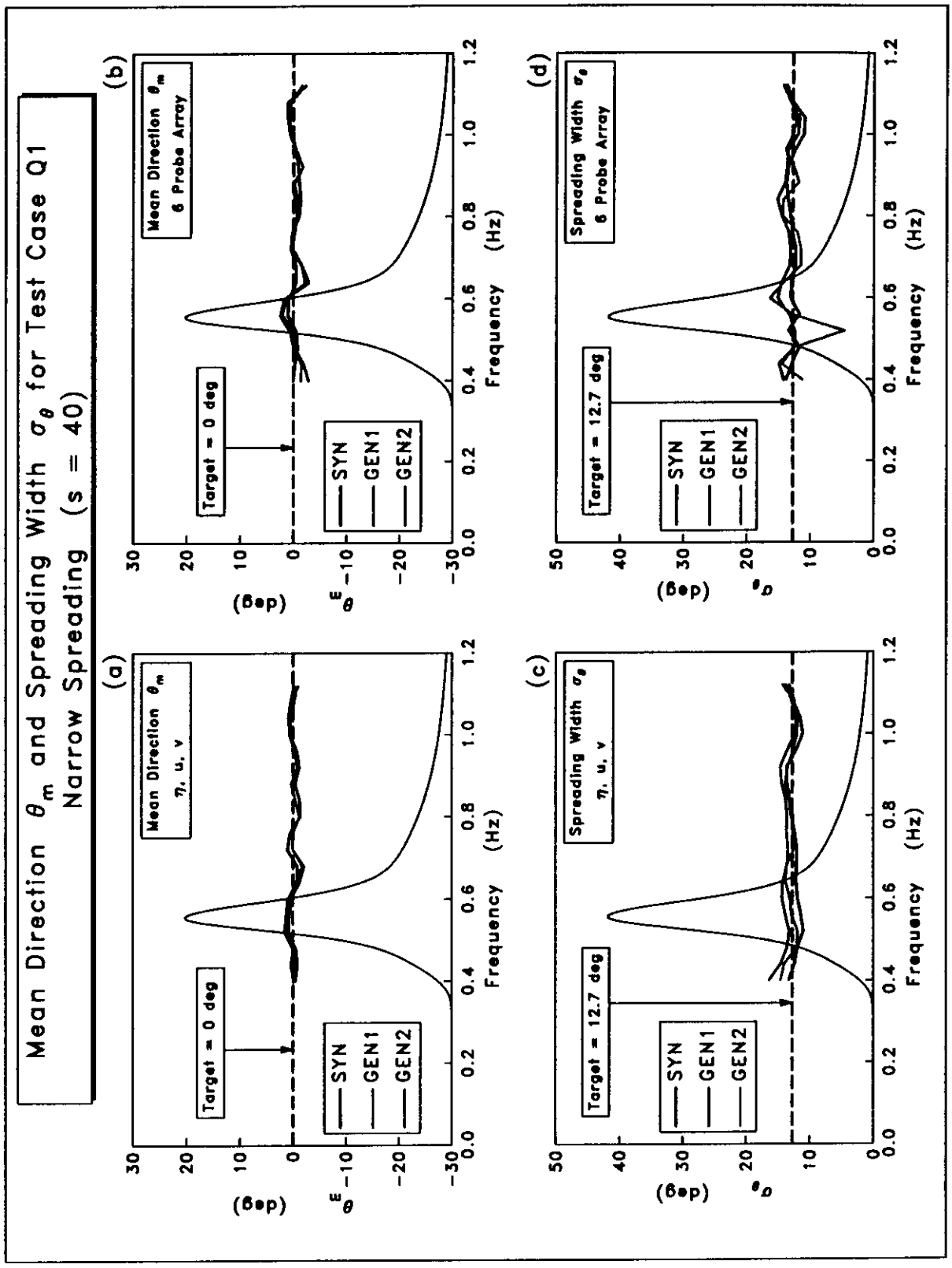

Figure 8: Mean wave direction $\theta_m(f)$ and spreading width $\sigma_\theta(f)$ computed by programs MEMVL and MEMWP using time series data from numerical simulations of Test Case Q1

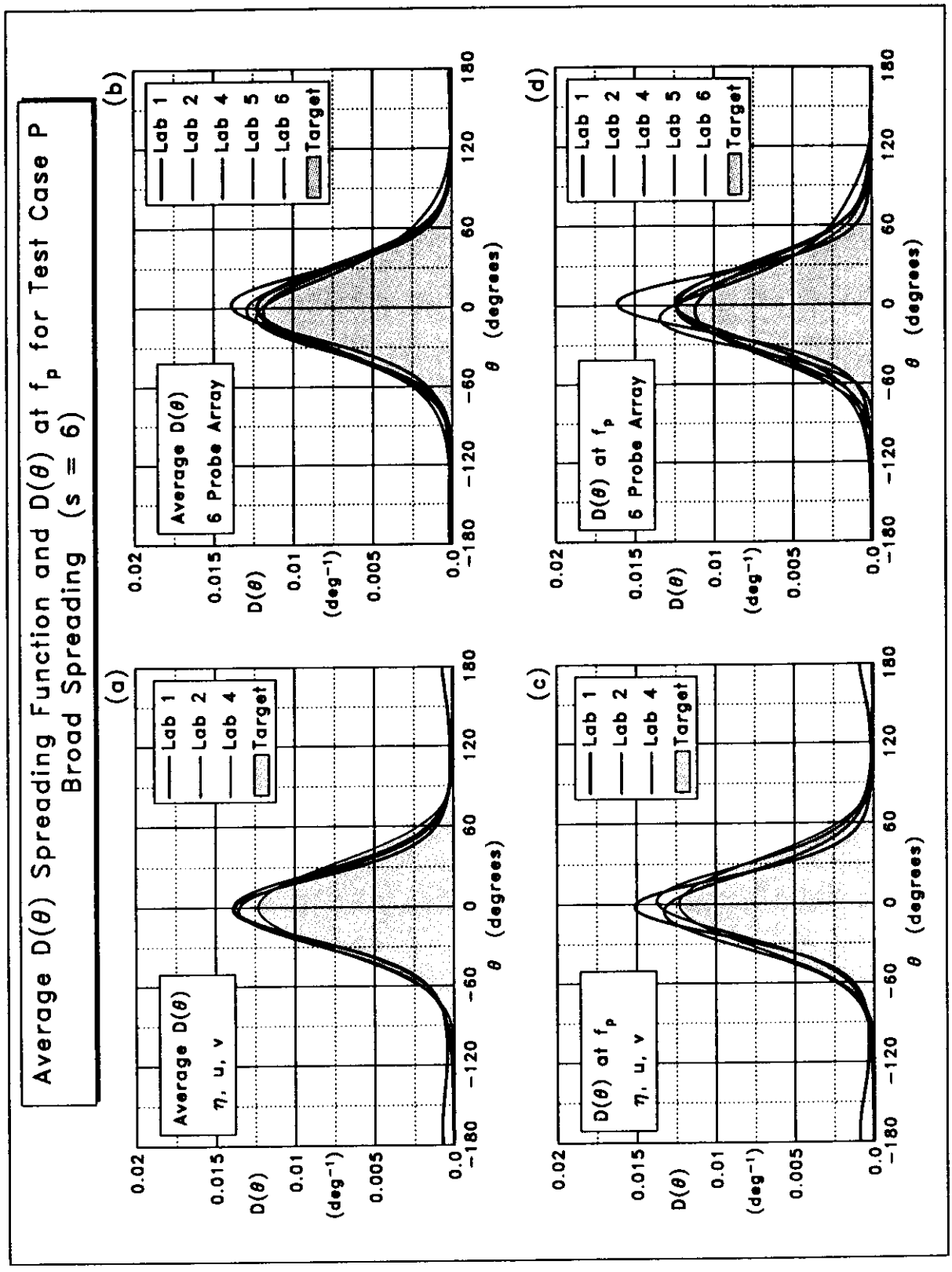

Figure 9: $D(\theta)$ spreading functions computed by programs MEMVL and MEMWP for waves generated in various laboratory basins for Test Case P

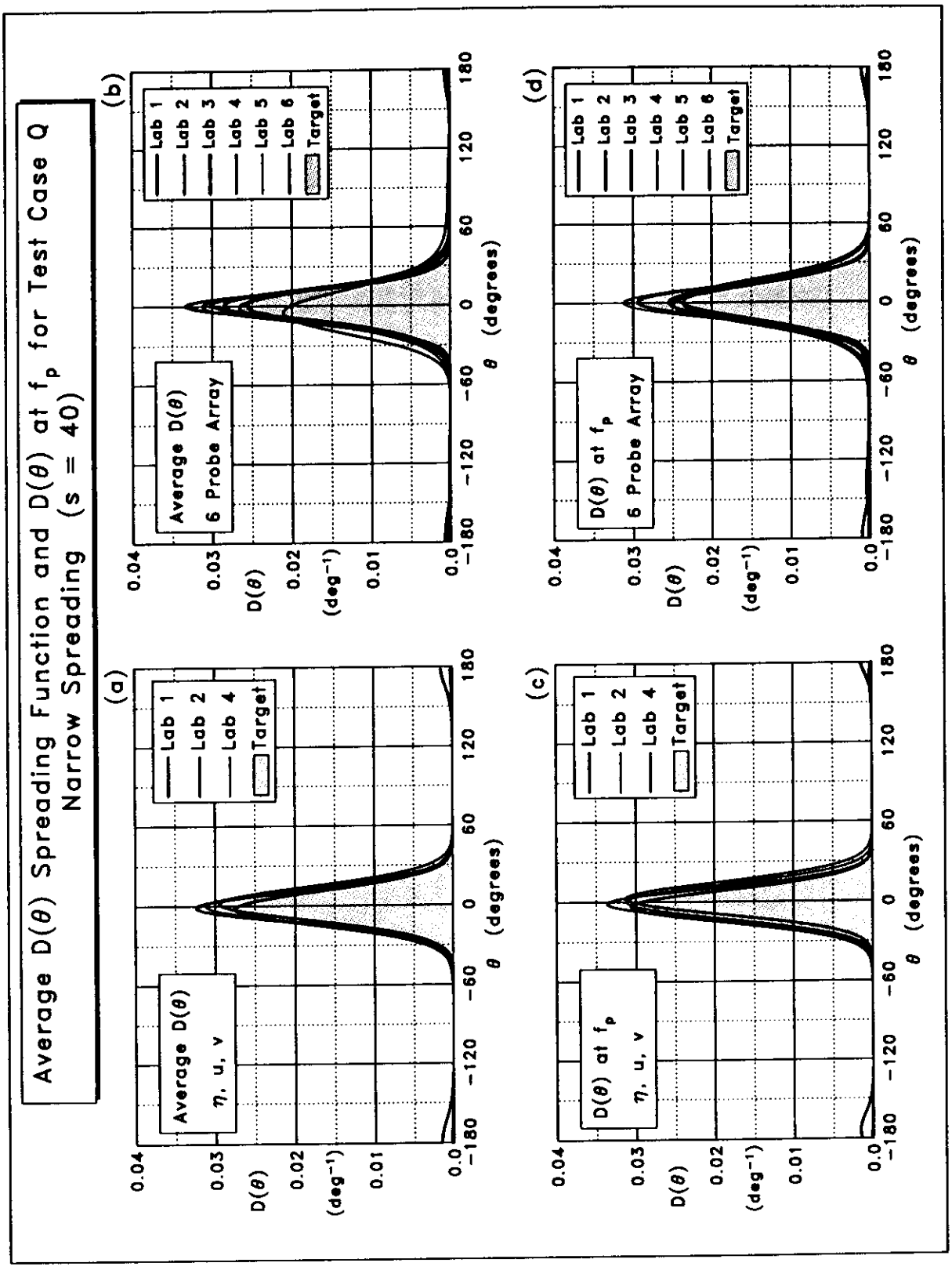

Figure 10: $D(\theta)$ spreading functions computed by programs MEMVL and MEMWP for waves generated in various laboratory basins for Test Case Q

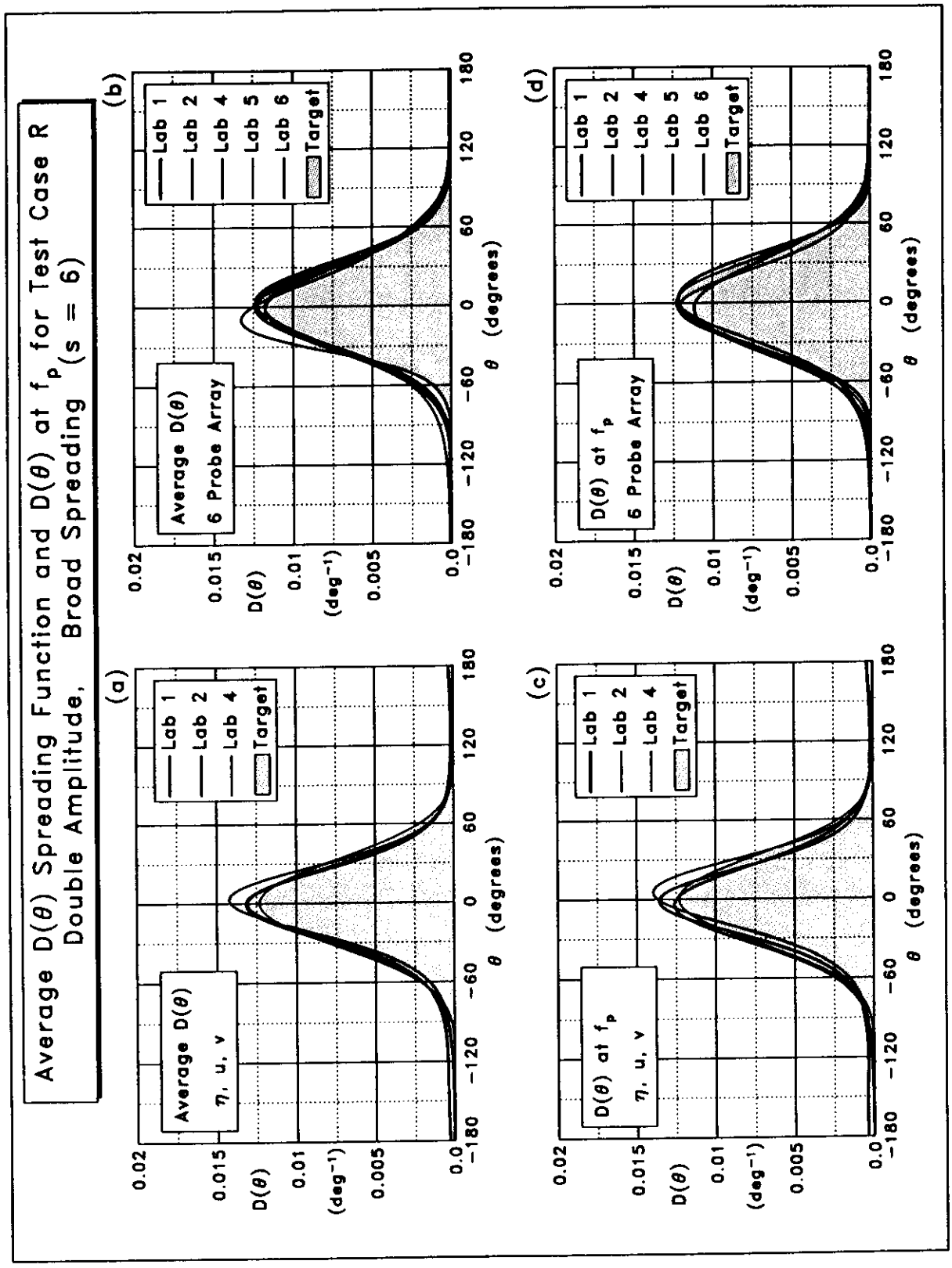

Figure 11: $D(\theta)$ spreading functions computed by programs MEMVL and MEMWP for waves generated in various laboratory basins for Test Case R

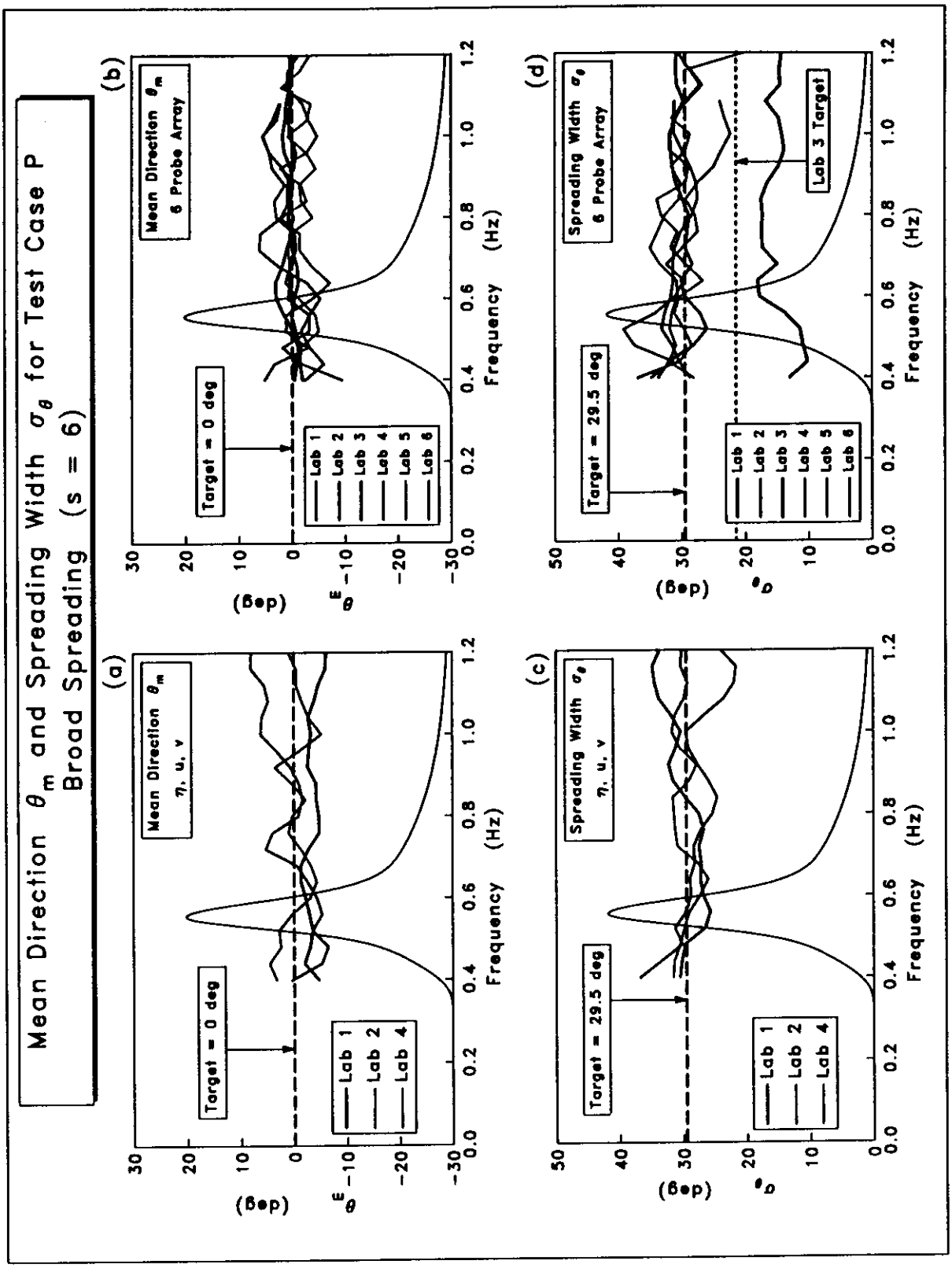

Figure 12: Mean wave direction $\theta_m(f)$ and spreading width $\sigma_\theta(f)$ computed by programs MEMVL and MEMWP for waves generated in various laboratory basins for Test Case P

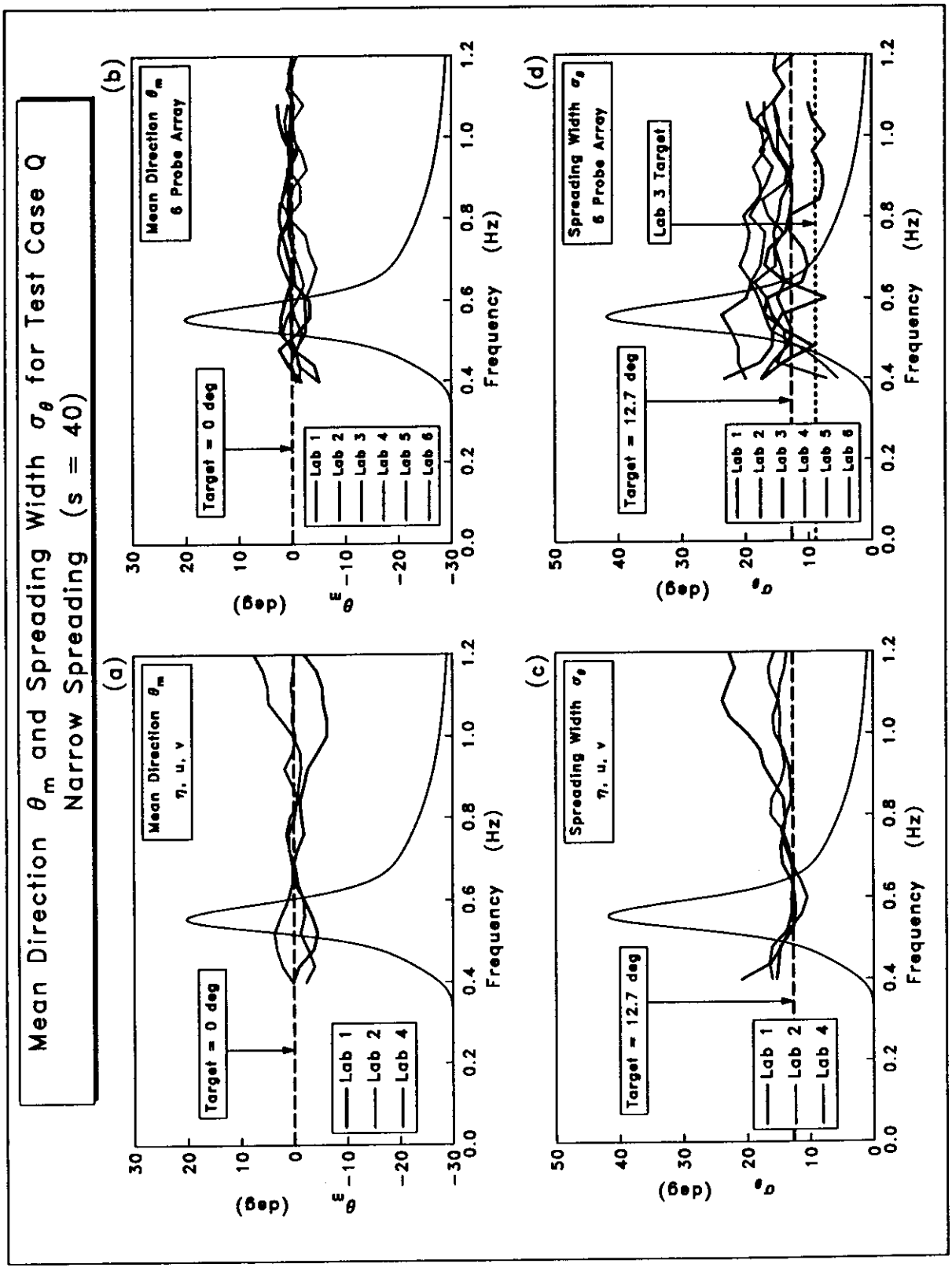

Figure 13: Mean wave direction $\theta_m(f)$ and spreading width $\sigma_\theta(f)$ computed by programs MEMVL and MEMWP for waves generated in various laboratory basins for Test Case Q

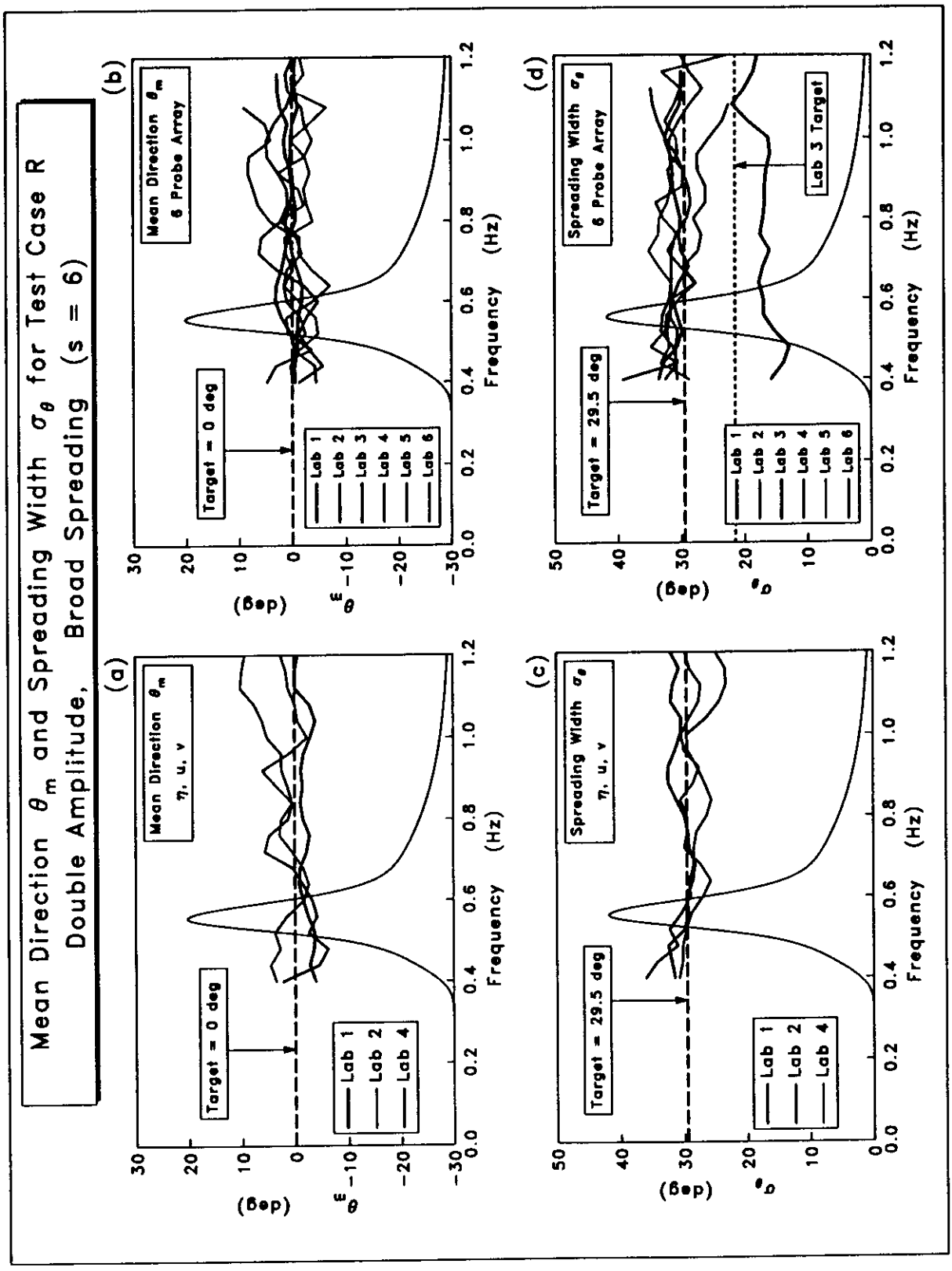

Figure 14: Mean wave direction $\theta_m(f)$ and spreading width $\sigma_\theta(f)$ computed by programs MEMVL and MEMWP for waves generated in various laboratory basins for Test Case R